J Mater Sci (2008) 43:5282–5290
DOI 10.1007/s10853-008-2790-z

Doping of lanthanum cobaltite by Mn: thermal, magnetic, and catalytic effect

Gina Pecchi · Claudia Campos · M. Graciela Jiliberto · Yanko Moreno · Octavio Peña

Received: 19 March 2008 / Accepted: 6 June 2008 / Published online: 24 June 2008

Abstract Great differences in crystallographic phases, magnetic properties, and catalytic activity were detected in lanthanum cobaltite and cobaltite modified with the insertion of 10 wt.% of Mn. Atomic absorption spectroscopy, BET area measurements, XRD analysis, TPR, and FT-IR suggest that the total insertion of manganese in the $LaCoO_3$ structure is successful. Thermal stability is reached for $LaCo_{0.90}Mn_{0.10}O_3$ up to 973 K without loss of the perovskite structure. The magnetic properties of the as-grown compounds are maintained after a first reduction process up to 723–773 K, while presence of segregated phases is observed after reduction at 973 K. The catalytic activity evaluated in the total combustion of acetyl acetate shows a decrease in the ignition temperature, i.e. an increase in the catalytic activity for the $LaCo_{0.90}Mn_{0.10}O_3$ perovskite. A significant enhancement in the catalytic activity expressed as intrinsic activity, mol m^{-2} h^{-1}, with the manganese substitution was found.

Introduction

Mixed oxides mixtures with perovskite/type structure, of general formula ABO_3, where A is a large cation and B is a small cation of the d-transition series, have been thoroughly investigated in the past decades [1–4]. Of great interest has been the investigation of the physico-chemical modifications when the A- and/or B-sites are substituted by cations of foreign metals, resulting in substantial changes in the magnetic [5], electric [6], and catalytic properties [7]. Among the particular aspects of this research, the catalytic activity is of great importance since it may lead to technical applications in the fields of oxide fuel cells or oxidation catalysts. Perovskite-mixed oxides based on Co or Mn are among the materials the most studied in this field because of low costs in comparison with noble metals catalysts and because of the possibility to present several oxidation states which may favor chemical bonds and physico-chemical interaction mechanisms.

It is by now well known that the partial substitution of the cation B by another one of similar oxidation state and ionic radius can improve the phase stability or enhance the perovskite's redox efficiency. These redox properties and the defect structure can be investigated and correlated by characterizing the solids with temperature programmed reduction (TPR) techniques, and X-ray diffraction (XRD) [8, 9]. In particular, some differences in the crystalline structure and transition temperature have been reported after substitution of 10 wt.% in the B-site [10], but not much information has been given on the interrelation between the phase stability and the catalytic activity of these materials.

On the other hand, magnetic properties are intimately related to the presence of mixed-valent cations, in particular manganese, because of its various oxidation states (Mn^{2+}, Mn^{3+}, Mn^{4+}). Substitution (or insertion) of manganese in perovskites may create favorable conditions for magnetic interactions through the oxygen orbitals, being sensitive to structural factors, to the substituent ratio or to cation and/or anion vacancies. As such, perovskite materials based on manganese and/or cobalt have been thoroughly studied in the past because of the very

G. Pecchi (✉) · C. Campos · M. G. Jiliberto · Y. Moreno
Facultad de Ciencias Químicas, Universidad de Concepción, Casilla 160-C, Concepcion, Chile
e-mail: gpecchi@udec.cl

O. Peña
Sciences Chimiques de Rennes, UMR 6226, CNRS, Université de Rennes 1, 35042 Rennes Cedex, France

interesting magnetoresistance properties [11, 12], but not much attention has been paid to the modifications of the magnetic properties with the catalytic activity, since redox effects will immediately affect the anionic network.

The case of the lanthanum cobaltite $LaCoO_3$ is particularly interesting, mainly from the point of view of its electronic properties [13] and as a total oxidation catalyst [14]. Two spin-state transitions are expected for the cobalt ion, from a low-spin to a high-spin configuration, via an intermediate spin-state. Then, the partial substitution of Co by a B cation may drastically modify its electronic structure and improve these important applications.

The present work was undertaken with the aim to determine the effects of doping, herein defined as a partial substitution (of the order of 10 wt.% or less), of isovalent transition-metal elements (Co by Mn) on the structure and physico-chemical properties of the lanthanum cobaltite $LaCoO_3$. Our main objective is to know the interrelation among the phase stability, the redox properties, and the magnetic interactions since any modification to the overall oxidation state of the cationic sublattice will immediately affect the anionic network, and hence, the catalytic activity. For this, samples of lanthanum cobaltite $LaCoO_3$ and 10%-substituted $LaCo_{0.90}Mn_{0.10}O_3$ have been prepared and subjected to reduction–oxidation cycles at two different temperatures in order to determine their phase stability, the catalytic activity, the oxidative efficiency and, at the same time, to evaluate the modifications of their magnetic properties.

Experimental

$LaCoO_3$ and $LaCo_{0.90}Mn_{0.10}O_3$ perovskites were prepared by the citrate method [15]. Stoichiometric amounts of an aqueous solution of nitrates of the corresponding metals were added to an aqueous solution of citric acid with a 10% excess over the number of ionic equivalents of cations. The resulting solution was stirred at room temperature and slowly evaporated at 343 K under vacuum in a rotary evaporator until gel formation is reached. Then this gel was dried in an oven, slowly increasing the temperature by 1 K min^{-1} up to 523 K and maintaining it overnight to yield a solid amorphous citrate precursor. The resulting powder was crushed and sieved to obtain the required particle size (<200 μm), then heated up to 973 K at a rate of 1 K min^{-1} and held in air at this working temperature for 6 h.

Characterization

Specific surface area

Specific areas were calculated using the BET method [16] from the nitrogen adsorption isotherms, recorded at the temperature of liquid nitrogen on a Micromeritics apparatus Model ASAP 2010. Prior to the adsorption measurements, samples were out-gassed at 10^{-6} torr at 423 K.

TPR cycles

TPR experiments were performed in a TPR/TPD 2900 Micromeritics system provided with a thermal conductivity detector (TCD). Samples of about 20 mg were placed in a U-shape quartz tube previously purged in a synthetic air stream of 50 mL/min at 773 K for 1 h and then cooled to room temperature. Reduction profiles were then recorded by passing a 5% H_2/Ar flow at a rate of 40 mL/min while heating at a rate of 10 K/min from ambient temperature to 1,173 K. Because the reduction profiles could be perturbed by experimental conditions [17, 18], the operating variables (initial amount of reducible oxides (So), total flow rate (V*), heating rate (β) and the initial H_2 concentration (Co)) were chosen in such a way to measure the line profile and peak position accurately [19, 20]. A cold-trap was placed just before the TCD of the instrument to remove the water from the exit stream.

X-ray powder diffraction

The XRD patterns of all calcined samples were obtained with nickel-filtered CuKα_1 radiation ($\lambda = 1.5418$ Å) using a Rigaku diffractometer controlled by a computer. XRD diffractograms were collected in the 2θ range of 5–80° in steps of 2°/min. Phase identification was carried out by comparison with the JCPDS-ICDD database cards.

Fourier transform infrared spectroscopy

Fourier transform infrared (FT-IR) spectra were recorded in a Nicolet Magna-IR 550 instrument, equipped with a quartz sample holder with KBr windows. The perovskites were dehydrated at 483 K and finely ground in an agate mortar with KBr to obtain a sample/KBr ratio 1/150.

Magnetic measurements

Magnetic measurements between 2 and 300 K were performed using a Quantum Design MPMS-XL5 SQUID susceptometer. Samples were first cooled under no applied field; then, an external d.c. field of 250 Oe was applied at 2 K and samples were warmed up while recording the magnetization (zero-field-cooled mode, ZFC). Once at the maximum temperature, samples were cooled down under the same applied field (field-cooled mode, FC). In this way, any irreversibility in the ZFC/FC magnetization cycle is due to an ordered state settled at $T = T_{rev} = T_c$.

Catalytic activity

The catalytic activity evaluation in the total combustion of acetyl acetate was performed in a conventional flow reactor at atmospheric pressure using an LHSV of 150 h^{-1}. In each experiment, 50 mg of catalysts diluted with 100 mg of silica as an inert was used. The activity was measured at different temperatures. The reactant mixture was fed into the reactor at 100 mL/min, measured at room temperature, and the temperature was linearly increased up to the required temperature, and then maintained constant for 30 min. Then, it was raised to a new isothermal temperature using the same heating rate (1 K min^{-1}). Several isothermal steps were performed until reaching complete conversion. The molar mixture used was $C_4H_8O_2$:O_2:He = 1:10:89. Reactor effluents were analyzed using an on-line gas chromatograph Hewlett Packard model HP 4890D with a TCD. Helium was used as a carrier gas and the column used was a Porapack S and a Supel Q plot 30 m and 0.53 mm.

Results and discussion

Specific area

The specific surface area of the cobaltite decreased from 13.0 to 9.5 m^2 g^{-1} upon the insertion of 10% Mn, before the redox reactions (Table 1). This result is indicative of an increase in the mean particle size and a low degree of crystallinity with the substitution of manganese on cobaltite. After the reduction–oxidation reactions, the specific surface areas were found to increase, as it will be discussed below.

TPR cycles

TPR cycles (TPR_1–TPR_2) were performed in order to study the perovskites' reducibility, which is a key parameter when studying the effect of manganese addition on the cobaltite stabilization. The procedure included the following steps: (i) a first reduction step under H_2/Ar flow up to 973 K (herein named as TPR_1); (ii) cooling in Ar flow to room temperature; (iii) oxidation in an O_2/He flow mixture up to 973 K; and (iv) a second reduction treatment (herein named as TPR_2) similar to step (i) once the sample was cooled to ambient temperature. This procedure was selected to study the perovskites' thermal stability under hydrogen. Figure 1 displays the TPR_1 and TPR_2 of cobaltite (Fig. 1a, c) and $LaCo_{0.90}Mn_{0.10}O_3$ (Fig. 1b, d). Differences in the $LaCoO_3$ and $LaCo_{0.90}Mn_{0.10}O_3$ reduction profiles are observed, where the two reduction peaks of the non-substituted cobaltite are larger and better defined, both for TPR_1 and TPR_2. The TPR_1 of the cobaltite presents two well-defined peaks, centered at 653 and 818 K, the larger one at the higher temperature. These results are in agreement with those reported for the cobaltite reduction by Marcos et al. [21] and Crespin and Keith [22]. They report an oxygen-deficient perovskite structure ($LaCoO_{3-\delta}$) at temperatures below 673 K. This result corresponds to the first reduction peak in TPR_1 for the cobaltite. The complete reduction of perovskite, with formation of La_2O_3, $La(OH)_3$, H_2O and Co^o, corresponds to the second reduction peak of TPR_1 at temperatures above 773 K. Another reduction mechanism, reported by Sis and Wirtz [23], points to the formation of intermediate products, such as cobalt spinels as well as manganese and lanthanum oxides. In order to explain the existence of an oxygen-deficient cobaltite, other authors have proposed a charge disproportionation of Co^{3+}, with Co^{2+} and Co^{4+} amounts of about 20% each [24]. Thanks to our milder conditions of synthesis and reduction, the XRD data (to be discussed below) do not show any presence of segregation. The total hydrogen consumption in the TPR profiles allows to calculate the extent of reduction of the perovskite structure. The H_2/(Co + Mn) molar ratio values of 4.2 and 4.0% corresponding to $LaCoO_3$ and $LaCo_{0.90}Mn_{0.10}O_3$, respectively, are indicative of the Co reduction in the perovskite structure. In the TPR_1 of $LaCo_{0.90}Mn_{0.10}O_3$ perovskite, two peaks are also detected, with almost no change in the one at the lowest temperature compared with the TPR_2 of the non-substituted cobaltite. This peak occurs at 647 K which, according to the literature, corresponds to the reduction of

Table 1 Specific surface, ignition temperature (T_{50}) and reaction rate referred to weight, atomic content, and surface area at conversion level lower <10% for cobaltite and $LaCo_{0.9}Mn_{0.1}O_3$ perovskite

	S_{BET} (m^2 g^{-1})	Ignition T_{50} (K)	Reaction rate at 503 K		
			mmol g^{-1} h^{-1}	mmol at $(Co + Mn)^{-1}$ h^{-1}	mmol m^{-2} h^{-1}
$LaCoO_3$–O_2 973 K	13.1	510	10.8	45.0	0.83
$LaCoO_3$–H_2 723 K	10.8	520	5.3	22.1	0.49
$LaCoO_3$–H_2 973 K	15.7	532	4.0	16.7	0.26
$LaCo_{0.9}Mn_{0.1}O_3$–O_2 973 K	9.5	505	12.2	51.3	1.28
$LaCo_{0.9}Mn_{0.1}O_3$–H_2 773 K	10.8	516	9.5	39.9	0.88
$LaCo_{0.9}Mn_{0.1}O_3$–H_2 973 K	16.5	518	8.2	34.5	0.50

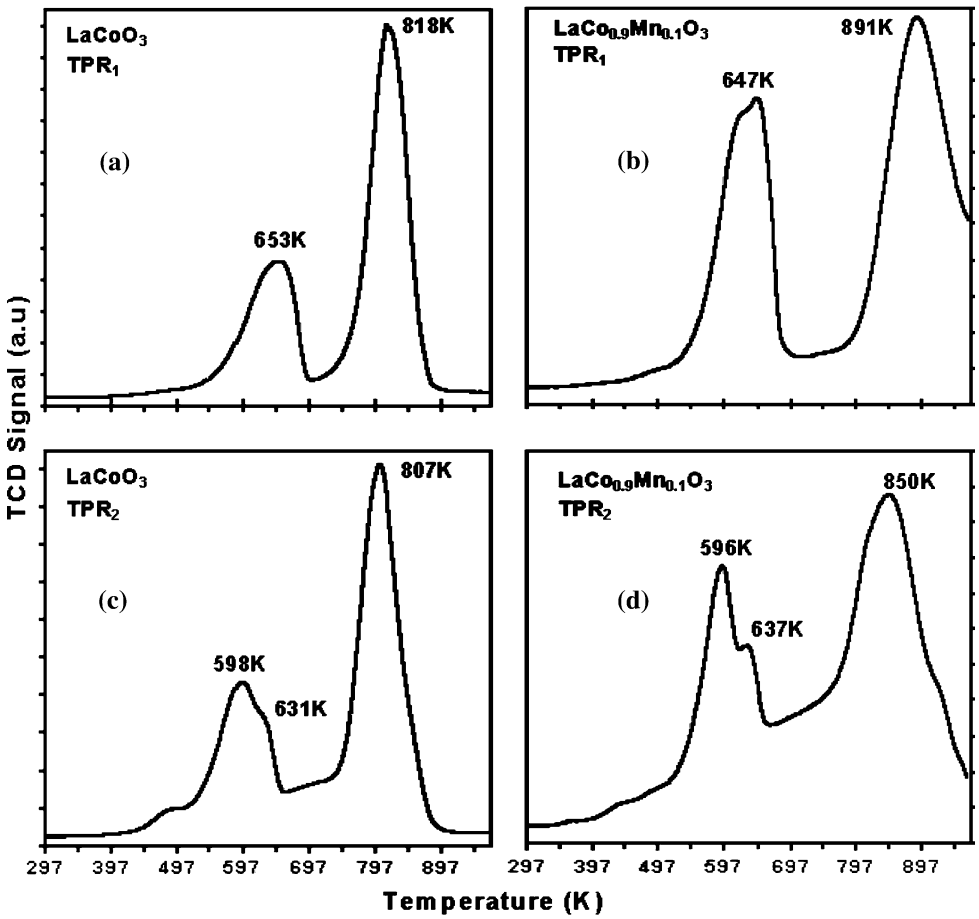

Fig. 1 TPR cycles. (**a**) TPR_1 of $LaCoO_3$; (**b**) TPR_1 of $LaCo_{0.9}Mn_{0.1}O_3$; (**c**) TPR_2 of $LaCoO_3$; (**d**) TPR_2 of $LaCo_{0.9}Mn_{0.1}O_3$

the network with the formation of oxygen-deficient perovskite. Since the reduction peaks are well defined, the effects can be studied independently. Thus, the study was extended, performing two TPRs separately but under identical conditions: up to 773 and up to 973 K. Therefore, three sets of data are presented in this study (Table 1): (i) as-grown samples calcined in air at 973 K for 2 h; (ii) samples annealed under H_2/Ar gas flow at 723 K (for $LaCoO_3$) or 773 K (for $LaCo_{0.90}Mn_{0.10}O_3$) corresponding to the samples after the first reduction peak; (iii) the same compositions after a H_2/Ar annealing at 973 K. Using XRD, FTIR, and magnetic properties, the structural changes after thermal treatment were studied and they are presented here below.

The similarities between the TPR_1 and TPR_2 for each one of the perovskites (Fig. 1) indicate that the original perovskite phase is restored after the reduction–oxidation cycles, in agreement with previous results reported for the cobaltite [22]. The completely restored perovskite structure through reversible reduction–oxidation cycles allows explaining the increase in the specific surface area of the regenerated perovskites compared with the original samples. Similar behavior has been reported for $LaRhO_3$ [25] and $PrCoO_3$ [26] perovskites.

X-ray diffraction

The XRD analysis was performed with the purpose to reveal the crystal structure and crystalline phases developed during the calcination step up to 973 K (O_2-973 K, as grown). Additionally, to study the effect of the Mn insertion on the thermal stability of the cobaltite in a reductor atmosphere and to determine if the first reduction peak in the TPR_1 (653 K) corresponds to an intermediate reduction. Thus, a reduction process was performed in hydrogen atmosphere up to 723 K and a diffractogram was recorded. The same procedure was performed with the second reduction peak, annealing processes at 973 K. Figure 2 displays the XRD patterns of the $LaCoO_3$ (Fig. 2a) and $LaCo_{0.9}Mn_{0.1}O_3$ (Fig. 2d) for the three annealing conditions: O_2-973 K, O_2-973 K/H_2-723 K (773 K for $LaCo_{0.90}Mn_{0.10}O_3$) and O_2-973 K/H_2-973 K. It can be seen that the as-grown cobaltite can be identified with the JCPDS 84-0848 pattern for $LaCoO_3$, which corresponds to a rhombohedral system, in agreement with the results reported in the literature [27, 28]. Two characteristic signals of this structure are observed: a doublet which appears at 2θ of 33° and the shoulder at 59°. The annealing processes modify the corresponding diffractograms, indicating

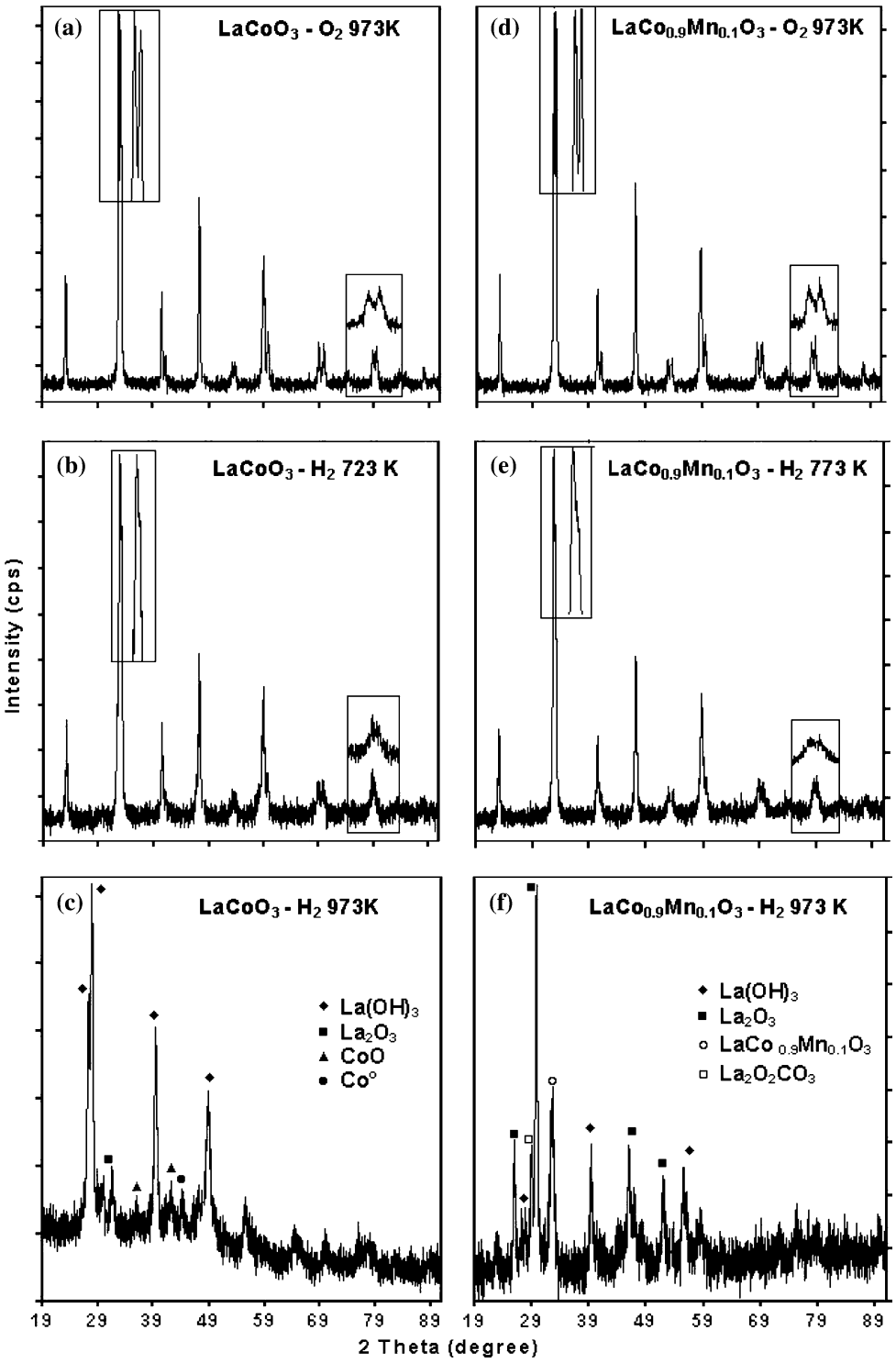

Fig. 2 XRD profiles for (**a**) $LaCoO_3$ as grown; (**b**) $LaCoO_3$ annealed under H_2/Ar at 723; (**c**) $LaCoO_3$ annealed under H_2/Ar at 973 K; (**d**) $LaCo_{0.9}Mn_{0.1}O_3$ as grown; (**e**) $LaCo_{0.9}Mn_{0.1}O_3$ annealed under H_2/Ar at 773; (**f**) $LaCo_{0.9}Mn_{0.1}O_3$ annealed under H_2/Ar at 973 K

changes in the structure. For both perovskites, the thermal stability in reductor atmosphere is quite acceptable for the treatment up to 723 K since the recorded diffractograms are practically identical to the respective calcined perovskites. A lower intensity of the diffraction lines indicates a lower crystallinity while the absence of extra lines indicates no segregated phases, thus maintaining the perovskite structure. The diffractogram of the cobaltite sample confirms the presence of a rhombohedral phase presenting diffraction lines which are coincident with the JCPDS 84-0848 pattern. This diffractogram presents signals characteristic for this structure, acute and intense at $2\theta = 33°$ while the signal at $2\theta = 47°$ is wider and weaker. Consequently, it is proposed that cobaltite's thermal stability in a

reductor atmosphere at temperatures below 723 K obeys to the reaction:

$$LaCoO_3 + \gamma H_2 \rightarrow LaCoO_{3-\delta} + \gamma H_2.$$

The presence of segregated phases was not observed for this sample. The extraction of oxygen transforms then the perovskite structure into an oxygen deficient one.

On the other hand, the annealing process up to 973 K presents drastic modifications of the diffractograms, which indicate the disappearance of the original structure and the appearance of new crystalline phases. The perovskite structure is completely lost because its most important diffraction peak at 2θ of 33° fully disappears and a large quantity of segregated phases appears, such as $La(OH)_3$ and La_2O_3 as well as $La_2O_2CO_3$, that is a mixture of oxide, hydroxide, and lanthanum carbonate. A peak at $2\theta = 41°$, corresponding to metallic cobalt, was also observed. The two bands at $2\theta = 38$ and 43° correspond to cobalt oxide (CoO); this is because cobalt is completely reduced to Co° above 773 K, and consequently it forms water vapor in a hydrogen-reductor atmosphere due to the extraction of oxygen from the network. Then, Co° is oxidized and forms CoO. Additionally, formation of $La_2O_2CO_3$ occurs because of the exposure to air. Consequently, for temperatures above 973 K, the equation representing the transformation process of the cobaltite perovskite's structure is:

$$LaCoO_3 + \gamma H_2 \rightarrow La_2O_3 + La(OH)_3 + Co^\circ + \gamma H_2O.$$

The formation of cobalt and lanthanum spinels detected in this perovskite was also reported by Crespin and Keith [22] and they are formed as a series of at least three reduction–oxidation cycles. Consequently, it can be concluded that the cobaltite maintains its rhombohedral structure after the first reduction process at 723 K and that the structure is lost after the reduction process at 973 K.

The diffractograms of the $LaMn_{0.1}Co_{0.9}O_3$ perovskite as grown and after annealing up to 773 and 973 K are shown in Fig. 2d–f. As before, and according to the literature [29], the first reduction peak of TPR_1 which appears at 647 K corresponds to the network reduction with the formation of the oxygen-deficient perovskite. This result is confirmed by the diffractogram of the sample annealed at 773 K, which corresponds quite well to the $LaCoO_3$ pattern. The crystallographic structure is partly maintained for $LaCo_{0.9}Mn_{0.1}O_3$ annealed at 973 K since the diffraction peaks at about $2\theta = 33°$, characteristic of the perovskite structure, are conserved. In addition, several diffraction lines appear at 2θ of 28 and 32°, identified as a mixture of $La(OH)_3$ and La_2O_3. The reason for these segregated phases is due to the structure reduction. Since La is present in a greater proportion, it has the capacity to form crystals that are X-ray observable. These results clearly show an enhancement of the thermal stability of the cobaltite substituted with 10% Mn. At temperatures greater than 773 K, the proposed reduction reaction is:

$$LaCo_{0.9}Mn_{0.1}O_3 + \gamma H_2 \rightarrow LaCo_{0.9}Mn_{0.1}O_{3-\delta} + La_2O_3 + La(OH)_3 + H_2O.$$

The non-detection of other segregated phases and the fact that the structure is partly maintained indicate that the extracted oxygen is preferentially converted into water.

FT-IR spectroscopy

Figure 3 presents the IR spectra for $LaCoO_3$ and $LaCo_{0.9}Mn_{0.1}O_3$ in the zones between 4,000 and 500 cm^{-1} for the three systems studied: O_2-973 K, O_2-973 K/H_2-723 K (773 K for $LaCo_{0.90}Mn_{0.10}O_3$), and O_2-973 K/H_2-973 K. The spectrum of the as-grown cobaltite presents a very intense band at 604 cm^{-1} with a shoulder at 563 cm^{-1}, which corresponds to the mode ν_1, an asymmetric enlargement of the B–O bond of the octahedral BO_6. The bands at 1,495 and 1,377 cm^{-1} correspond to the vibration mode ν_3 of the CO_3^{2-} groups of the O–C–O bond. The higher intensity of this band implies that the samples present segregated phases in the form of carbonates. The wide band at 3,600 cm^{-1} is associated to the enlargement of the water's O–H bond, due to exposure to air and environmental humidity. The IR spectra of the annealed cobaltite at 973 K (Fig. 3b) presents notable differences: the band corresponding to the mode ν_1 disappears and the OH flexion vibrations appear at 647 cm^{-1} for the species $La(OH)_3$, indicating the presence of the species $La(OH)_3$ and $La_2O_2CO_3$. It can be observed that the three spectra present carbonate bands, but these are more intense in the perovskite annealed at 973 K. This result confirms the XRD data, which show that the cobaltite treated at 973 K in H_2 is completely reduced, loses the perovskite structure, and the predominant phase is lanthanum hydroxide.

In the IR spectrum of the $LaCo_{0.9}Mn_{0.1}O_3$ perovskite annealed at 973 K, the carbonate band is observed but at a lower intensity than observed in cobaltite, which implies less phase segregation due to the reduction. The vibration band of OH enlargement appears with less intensity, which implies a lower hydroxide formation. In the substituted perovskite, the band corresponding to the octahedral MO_6 is masked by the OH flexion that appears in the same region [30].

Consequently, the samples' stability in hydrogen atmosphere characterized by XRD and FT-IR indicates that the incorporation of Mn in the cobaltite increases the structural stability since the hydroxide and the carbonate band intensities diminish. XRD results indicate that the reduction reaction produces a mixture of La_2O_3 and $La(OH)_3$. The IR results show that $La(OH)_3$, as the predominant species, forms $La_2O_2CO_3$ due to air exposure.

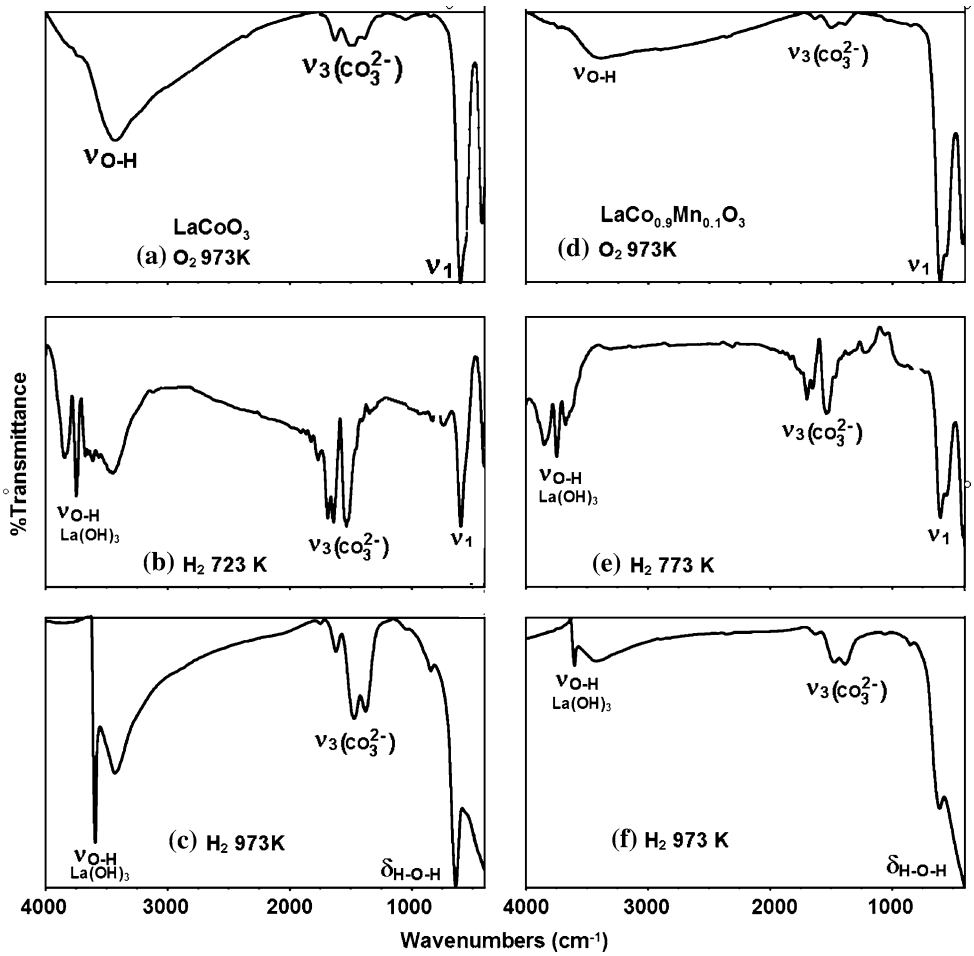

Fig. 3 FTIR spectra for (**a**) $LaCoO_3$ as grown; (**b**) $LaCoO_3$ annealed under H_2/Ar at 723; (**c**) $LaCoO_3$ annealed under H_2/Ar at 973 K; (**d**) $LaCo_{0.9}Mn_{0.1}O_3$ as grown; (**e**) $LaCo_{0.9}Mn_{0.1}O_3$ annealed under H_2/Ar at 773; (**f**) $LaCo_{0.9}Mn_{0.1}O_3$ annealed under H_2/Ar at 973 K

Magnetic properties

Figure 4 shows the thermal variation of the magnetic susceptibility (defined as the ratio M/H) for $LaCoO_3$ and $LaCo_{0.90}Mn_{0.10}O_3$. Three sets of data are shown: as-grown samples calcined in air at 973 K for 2 h (panels a and d); samples annealed under H_2/Ar gas flow at 723–773 K (b and e); the same compositions after an H_2/Ar annealing at 973 K.

The ZFC magnetization of as-grown samples (open circles; upper panels) can be described in terms of magnetic-electronic transitions, as reported in the lanthanum cobaltite $LaCoO_3$, for which well-defined anomalies were observed near 110 and 500 K [31]. In the usual $3d^6$ configuration for Co^{3+}, a low-spin (LS; $S = 0$) and a high-spin (HS; $S = 2$) states are expected, but an intermediate-spin state (IS; $S = 1$) has been proposed to explain thermally activated LS to IS and IS to HS transitions [31–33]. On the other hand, extremely low doping may transform diamagnetic $LaCoO_3$ into a paramagnetic compound ($S \cong 1.5$) with a spin-glass transition at $T_{SG} \sim 25$ K [34]. This situation is found in our as-grown sample $LaCoO_3$ (Fig. 4), where the electronic transition occurs at $T_{cusp} = 25$, and for which the paramagnetic state is characterized by an effective moment of 3.42 μ_B.

The overall behavior of $LaCo_{0.90}Mn_{0.10}O_3$ can be discussed using two different approaches. The first one is that Mn enters the solid solution as a trivalent cation, Co^{3+}, triggering antiferromagnetic Mn^{3+}–Co^{3+} interactions. The second approach is that Mn enters as tetravalent ion, transforming a cobalt ion into Co^{2+}, and promoting ferromagnetic Co^{2+}–Mn^{4+} interactions. Although the first possibility looks quite plausible, the second one is experimentally correct, as we reported on the solid solution $LaCo_xMn_{1-x}O_3$ ($0.0 \leq x \leq 1.0$) [35]. For the $LaCo_{0.90}Mn_{0.10}O_3$ sample under study, the amount of Co^{2+}/Mn^{4+} pairs is low (10 wt.% of manganese ions), so ferromagnetic interactions are weak compared to the predominant spin-state transition characteristic of the cobaltite $LaCoO_3$. By analogy with the slightly-doped lanthanum manganite $(La^{3+},Sr^{2+})MnO_3$, which is the archetype of a canted-spin AF state (ferromagnetic planes coupled by an antiferromagnetic interaction [36, 37]), we may argue that the $LaCo_{0.90}Mn_{0.10}O_3$ case presents a similar behavior and can be described as a canted-spin antiferromagnet.

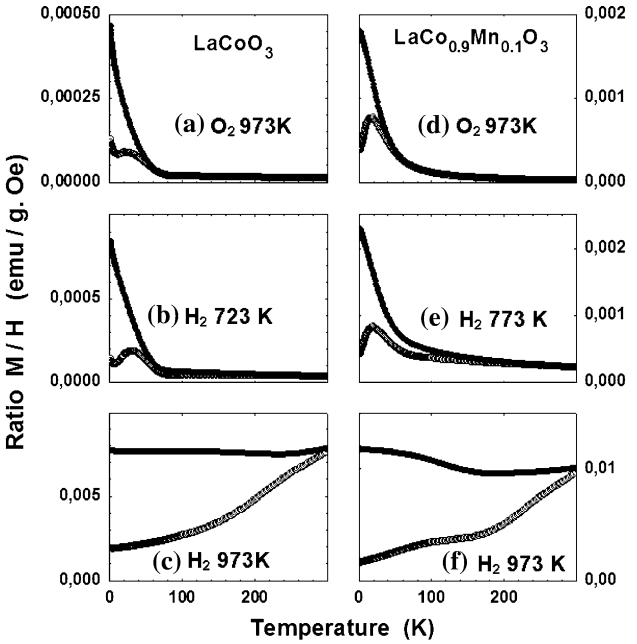

Fig. 4 Magnetization cycles measured under 250 Oe (ZFC: open symbols; FC: filled symbols) for (**a**) $LaCoO_3$ as grown; (**b**) $LaCoO_3$ annealed under H_2/Ar at 723; (**c**) $LaCoO_3$ annealed under H_2/Ar at 973 K; (**d**) $LaCo_{0.9}$ $Mn_{0.1}O_3$ as grown; (**e**) $LaCo_{0.9}$ $Mn_{0.1}O_3$ annealed under H_2/Ar at 773; (**f**) $LaCo_{0.9}$ $Mn_{0.1}O_3$ annealed under H_2/Ar at 973 K

Examining the effects of the reduction annealing (Fig. 4c, f), it is readily seen that the high thermal process at 973 K decomposes both samples, resulting in a large percentage of cobalt oxide or metallic cobalt, with magnetic ordering temperatures well above room temperature. Superparamagnetic effects with high blocking temperatures may also exist and attributed to nanoclusters of Co formed during the reduction, but the large difference in the *Y*-scales between panels a–d and c–f leads us to privilege the presence of segregated phases of metallic cobalt, as shown by the XRD data. This has been also reported by Sis and Wirtz [23] for different reduction rates; that is, for samples resulting from a reduction reaction of the type $LaCoO_3 \rightarrow LaCo_xO_{3-y} + (1 - x)Co + \frac{1}{2}yO_2$.

In contrast, samples annealed at moderate temperatures (723–773 K; panels b and e) under H_2/Ar gas flow behave very similar to the as-grown specimens, thus confirming that the $LaCoO_3$ and $LaCo_{0.90}Mn_{0.10}O_3$ compositions are quite stable under these reduction conditions, in good agreement with XRD results. Minute amounts of cobalt phases (not detected by XRD) may appear in $LaCo_{0.90}Mn_{0.10}O_3$ after annealing at 773 K, since T_{rev} increases quite anomalously from about 60 up to 170 K; while for the $LaCoO_3$ sample annealed at 723 K, T_{rev} stays relatively constant (62 and 70 K, for the as-grown and the annealed sample, respectively).

Catalytic activity

The as-grown $LaCoO_3$ and $LaCo_{0.90}Mn_{0.10}O_3$, calcinated at O_2-973 K, and the hydrogen-treated perovskites were tested in the total acetyl acetate combustion in a flow reactor under an excess of oxygen. CO_2 and H_2O were obtained as complete oxidation products, while the intermediate oxidation products (acetic acid, ethanol, and acetaldehyde) were detected only as traces. The catalytic activity is given in Table 1, informed as ignition temperature T_{50} (defined as the temperature required to obtain 50% conversion) and the reaction rate evaluated at 503 K and under a low conversion level (<10%), referred to catalyst weight (mmol g^{-1} h^{-1}), (Co + Mn) atoms (mmol at^{-1} h^{-1}) and catalyst surface (mmol m^{-2} h^{-1}). It can be seen that upon the insertion of Mn in the cobaltite, a decrease in the ignition temperature and an increase in the reaction rate are detected, indicative of a better catalytic activity. Therefore it can be concluded that the original $LaCoO_3$ activity increases when a small fraction of manganese substitutes cobalt.

On the other hand, a decrease in the catalytic activity is detected after the thermal treatment under reduction conditions, as seen in Table 1 for all reduced samples compared to the original products. This result can be explained considering a partial loss of the perovskite structure, as discussed previously.

The highest catalytic activity corresponds to $LaCo_{0.90}Mn_{0.10}O_3$–O_2 973 K, which has the lowest ignition temperature and the highest reaction rate. This noticeable increase could be explained as if the Mn ion enters the solid solution as a trivalent cation, so the charge equilibrium stays unchanged, with cobalt as Co^{3+}. However, an additional mechanism may occur, such as the charge redistribution $Mn^{+3} + Co^{+3} \rightarrow Mn^{+4} + Co^{+2}$. In this case, small amounts of tetravalent Mn are present, since double-exchange magnetic interactions are not negligible, as seen in Fig. 4d. Therefore, it is proposed that the higher catalytic activity is due to the presence of the redox couple Mn^{4+}/Co^{2+}.

The values of surface area do not vary significantly (Table 1), as it may be expected from the increase in the temperature for hydrogen treatment (larger crystallites sizes, agglomeration of particles, or grain growth, for instance). This behavior can be explained considering that the segregated oxides phases formed during the hydrogen treatment remain in a highly dispersed state. Such a loss of the perovskite structure is intimately related to the observed decrease in the catalytic activity and to the increase in the intermediate oxidation products. Finally, it was found that under the applied experimental conditions, for all the studied systems, the total conversion is achieved at temperatures below 540 K.

Conclusions

Perovskites having moderate specific areas have been obtained from the citrate route and the effect of the insertion of 10 wt.% of Mn on the thermal stability and catalytic activity in $LaCoO_3$ was studied. Based on the XRD, TPR, and FT-IR data, which showed that segregated phases formed under high temperature reduction conditions (such as hydroxides and carbonates of the type La_2O_3, $La(OH)_3$ or $La_2O_2CO_3$, or mixtures of them) are greatly diminished in the substituted perovskite, we may conclude on a significant enhancement of the structural stability in a reductor atmosphere when 10 wt.% Mn is incorporated into the original cobaltite. A noticeable improvement of the catalytic activity (expressed as mmol m^{-2} h^{-1}) after the manganese substitution on cobaltite was additionally found and explained by the incorporation of Mn ion as tetravalent ion, Mn^{4+}, transforming a cobalt ion into Co^{2+}. The magnetic properties of the as-grown compounds (spin transition, in the cobaltite, and canted-spin antiferromagnetism, for the 10%-substituted compound) are maintained after reduction at moderate temperatures of 723–773 K. At higher reduction temperatures (973 K) large amounts of cobalt impurities are created which dominate the magnetic properties of the original perovskite.

Acknowledgement The authors thank CONICYT (Fondecyt Grant 1060702).

References

1. O'Connell M, Norman AK, Hüttermann CF, Morris MA (1999) Catal Today 47:123. doi:10.1016/S0920-5861(98)00291-0
2. Tejuca LJ, Fierro JLG (eds) (1993) Properties and applications of perovskite-type oxides. Dekker, New York
3. Voorhoeve JH (1997) In: Burton HH, Garten RL (eds) Advanced materials in catalysis. Academic Press, New York, p 127
4. Hirusta S, Pina MP, Melendez M, Santamaría J (1998) Catal Lett 54:69. doi:10.1023/A:1019003216521
5. Peña O, Antunes AB, Martinez G, Gil V, Moure C (2007) J Magn Magn Mater 310:159. doi:10.1016/j.jmmm.2006.08.004
6. Chiba R, Yoshimura F, Sakurai Y (1999) Solid State Ionics 1–2:281. doi:10.1016/S0167-2738(99)00222-2
7. Pecchi G, Reyes P, Zamora R, Campos C, Cadús LE, Barbero BP (2008) Catal Today 133–135:420
8. Provendier H, Petit C, Estournes C, Libs S, Kienemann A (1999) Appl Catal Gen 180:163. doi:10.1016/S0926-860X(98)00343-3
9. Barbero BP, Andrade Gamboa J, Cadús LE (2006) Appl Catal B Environ 65:21. doi:10.1016/j.apcatb.2005.11.018
10. Inaba H, Hayashi H, Suzuki M (2001) Solid State Ionics 1–2:99. doi:10.1016/S0167-2738(01)00904-3
11. Rao CNR, Raveau B (eds) (1998) Colossal magnetoresistance charge ordering and related properties of manganese oxides. World Scientific, Singapore
12. Tokura Y (2000) Colossal magnetoresistive oxides. Gordon & Breach, New York
13. Kojima I, Adachi H, Yasumori I (1983) Surf Sci 130:50. doi:10.1016/0039-6028(83)90259-5
14. Spiniccia R, Tofanaria A, Faticantib M, Pettitib I, Porta P (2001) J Mol Catal A 176:247
15. Courty P, Ajot H, Marcilly C, Delmon B (1973) Power Technol 7:21. doi:10.1016/0032-5910(73)80005-1
16. Brunauer S, Emmett PH, Teller E (1938) J Am Chem Soc 60:309. doi:10.1021/ja01269a023
17. Vasanthacharya NY, Ganguly P, Rao CNR (1984) J Solid State Chem 53:140. doi:10.1016/0022-4596(84)90237-8
18. Chainani A, Sarma DD, Das I, Sampathkumaran EV (1996) J Phys Condens Matter 8:L631. doi:10.1088/0953-8984/8/43/001
19. Monti DAM, Baiker A (1983) J Catal 83:323. doi:10.1016/0021-9517(83)90058-1
20. Mallet P, Caballero A (1988) J Chem Soc Faraday Trans 84:2369. doi:10.1039/f19888402369
21. Marcos J, Buitrago G, Lombardo A (1987) J Catal 105:95. doi:10.1016/0021-9517(87)90011-X
22. Crespin M, Keith W (1981) J Catal 69:359. doi:10.1016/0021-9517(81)90171-8
23. Sis L, Wirtz G (1973) J Appl Phys 44:1. doi:10.1063/1.1662195
24. Yang M, Zhong Y, Liu Z-K (2007) Solid State Ionics 178:1027. doi:10.1016/j.ssi.2007.04.014
25. Olivari AOM, Peña MA, Tascon JM, Tejuca LG (1988) J Mol Catal 45:355. doi:10.1016/0304-5102(88)80067-1
26. Fierro JLG, Peña MA, Tejuca LG (1988) J Mater Sci 23:1018. doi:10.1007/BF01154005
27. Merino N, Barbero B, Ruiz P, Cadús L (2006) J Catal 240:11. doi:10.1016/j.jcat.2006.03.020
28. Bedel L, Roger A, Estournes C, Kiennemann A (2003) Catal Today 100:207. doi:10.1016/S0920-5861(03)00388-2
29. Koponen MJ, Suvanto M, Kallinen K, Kinnunen T-JJ, Harkonen M, Pakkanen TA (2006) Solid State Sci 8:450. doi:10.1016/j.solidstatesciences.2005.11.008
30. Davydov A (1990) Infrared spectroscopy of adsorbed species on the surface of transition metal oxides, chap 1. Wiley, England
31. Asai K, Yoneda A, Yokokura O, Tranquada JM, Shirane G, Kohn K (1998) J Phys Soc Jpn 67:290 and references therein. doi:10.1143/JPSJ.67.290
32. Fujine Y, Fujishiro H, Kashiwada Y, Hejtmanek J, Ikebe M (2005) Physica B (Amsterdam) 359–361:1360. doi:10.1016/j.physb.2005.01.411
33. Motin Seikh MD, Sudheendra L, Narayana C, Rao CNR (2004) J Mol Struct 706:121. doi:10.1016/j.molstruc.2004.03.058
34. Hejtmánek J, Jirák Z, Knížek K, Maryško M, Veverka M, Fujishiro H (2004) J Magn Magn Mater 272–276:e283. doi:10.1016/j.jmmm.2003.12.679
35. Pecchi G, Campos C, Peña O, Cadus LE (2008) J Mol Cat A Chem 282:158. doi:10.1016/j.molcata.2007.12.022
36. Wollan EO, Koehler WC (1955) Phys Rev 100:545. doi:10.1103/PhysRev.100.545
37. Kawano H, Kajimoto R, Kubota M, Yoshikawa H (1996) Phys Rev B 53:2202. doi:10.1103/PhysRevB.53.2202